Journal of Hydrology 538 (2016) 539–550

Contents lists available at ScienceDirect

Journal of Hydrology

journal homepage: www.elsevier.com/locate/jhydrol

Predicting available water of soil from particle-size distribution and bulk density in an oasis–desert transect in northwestern China

Danfeng Li [a], Guangyao Gao [a,b], Ming'an Shao [c,*], Bojie Fu [a,b]

[a] State Key Laboratory of Urban and Regional Ecology, Research Center for Eco-Environmental Sciences, Chinese Academy of Sciences, Beijing 100085, China
[b] Joint Center for Global Change Studies, Beijing 100875, China
[c] Key Laboratory of Ecosystem Network Observation and Modeling, Institute of Geographic Sciences and Natural Resources Research, Chinese Academy of Sciences, Beijing 100101, China

ARTICLE INFO

Article history:
Received 21 January 2016
Received in revised form 21 April 2016
Accepted 22 April 2016
Available online 30 April 2016
This manuscript was handled by Corrado Corradini, Editor-in-Chief, with the assistance of Juan V. Giraldez, Associate Editor

Keywords:
Soil water characteristic curve
Soil available water
Pedotransfer functions
Oasis–desert transect

SUMMARY

A detailed understanding of soil hydraulic properties, particularly the available water content of soil, (AW, $cm^3\ cm^{-3}$), is required for optimal water management. Direct measurement of soil hydraulic properties is impractical for large scale application, but routinely available soil particle-size distribution (PSD) and bulk density can be used as proxies to develop various prediction functions. In this study, we compared the performance of the Arya and Paris (AP) model, Mohammadi and Vanclooster (MV) model, Arya and Heitman (AH) model, and Rosetta program in predicting the soil water characteristic curve (SWCC) at 34 points with experimental SWCC data in an oasis–desert transect (20 × 5 km) in the middle reaches of the Heihe River basin, northwestern China. The idea of the three models emerges from the similarity of the shapes of the PSD and SWCC. The AP model, MV model, and Rosetta program performed better in predicting the SWCC than the AH model. The AW determined from the SWCCs predicted by the MV model agreed better with the experimental values than those derived from the AP model and Rosetta program. The fine-textured soils were characterized by higher AW values, while the sandy soils had lower AW values. The MV model has the advantages of having robust physical basis, being independent of database-related parameters, and involving subclasses of texture data. These features make it promising in predicting soil water retention at regional scales, serving for the application of hydrological models and the optimization of soil water management.

1. Introduction

Reasonable management of the soil water content status is crucial for plant growth and crop production in arid and semi-arid regions (Lawes et al., 2009; Hosseini et al., 2016). The soil available water, AW ($cm^3\ cm^{-3}$), is the amount of water released between in situ field capacity and the permanent wilting point. To determine AW, the pressure-based values of field capacity and wilting point are usually derived from the soil water characteristic curve (SWCC). This property measures the capability of soil to retain water, and reflects the effects of textural composition, mineralogy, soil structure, organic matter content and management practices (Arya et al., 2008). A quantitative and precise estimation of the SWCC is required in many hydrological models and is essential for a wide range of applications, such as soil and water conservation, irrigation scheduling, solute transport, and plant stress and growth (Ramos et al., 2014).

Direct measurement of the SWCC are always preferred in a small area, but laboratory procedures to determine it are time-consuming and costly, measuring it for large-scale regions at a fine spatial resolution is impractical (Gijsman et al., 2003). Indirect estimation of the SWCC from routinely available soil properties is simply one of the most feasible alternatives (Soet and Stricker, 2003; Ramos et al., 2014; Arya and Heitman, 2015). Particle-size distribution (PSD) is a basic property of mineral soils and can be measured easily and quickly. Using PSD, alone or in combination with bulk density and soil organic matter content, as surrogate data is attractive to predict selected points on the SWCC or the entire SWCC (Arya et al., 1999; Skaggs et al., 2001; Ramos et al., 2014; Jensen et al., 2015).

Current indirect methods for the SWCC estimation are classified into empirical, semi-physical, and conceptual methods (Schaap et al., 2004; Arya and Heitman, 2015). Following an empirical approach, a considerable number of pedotransfer functions (PTFs)

* Corresponding author. Tel.: +86 10 64889270.
E-mail address: shaoma@igsnrr.ac.cn (M. Shao).

http://dx.doi.org/10.1016/j.jhydrol.2016.04.046
0022-1694/

have been developed (Nemes et al., 2006; Bayat et al., 2013; Ghanbarian et al., 2015). Overviews of the current status of PTF approaches have been given by Wösten et al. (2001) and Gijsman et al. (2003). Pachepsky et al. (2015) comprehensively summarized the trends in PTF development and in input and output data, and methods to build PTFs. Various PTFs are usually given in the form of either a tabulation (Schaap and Leij, 1998; Soet and Stricker, 2003; Al Majou et al., 2008) or continuous functions (Wösten et al., 1999; Nemes and Rawls, 2006; Bayat et al., 2013; Haghverdi et al., 2015) to predict either a single point on the SWCC (Skaggs et al., 2001; Ramos et al., 2014) or parameters for the entire SWCC (Schaap et al., 2001). For example, the PTFs in the Rosetta program allow the estimation of parameters of van Genuchten equation for describing SWCC (van Genuchten, 1980) using limited (textural classes only) to more extended (texture, bulk density, and one or two water retention points) input data (Schaap et al., 2001). The reliability of PTFs can be hindered by the mismatch in measurements of data for developing the functions. The utility of PTFs may be limited to the environmental conditions the original data were collected and can be compromised by the mismatch in measurement times (Pachepsky et al., 2015). The application of regional PTFs has to be adapted to the particular situation under consideration (Wösten et al., 2001; Gijsman et al., 2003; Botula et al., 2012; Antinoro et al., 2014).

The semi-physical models provide conceptual insights into the physical relationship between soil particle size and pore size. These models are developed based on the close similarity between the shapes of PSD and pore size distribution (Arya and Paris, 1981; Arya et al., 1999; Hayashi et al., 2006; Hwang and Choi, 2006). A significant contribution, the AP model, was made by Arya and Paris (1981). In this semi-physical approach, pore radii were determined by scaling the pore lengths of cubic close-packed assemblages with spherical particles to those of the natural structure. Researchers thereafter have suggested that the SWCC prediction by the AP model would improve if the scaling parameter (α) were formulated as a varying rather than a constant value over soil particle ranges and textural classes (Basile and D'Urso, 1997; Arya et al., 1999; Vaz et al., 2005). The AP model has been progressively modified and used to predict SWCC. Arya et al. (1999) expressed the α values by logistic growth and linear fitting equations, which improved the SWCC estimation for 23 soils from the UNSODA hydraulic properties database (Leij et al., 1996). Antinoro et al. (2014) found that SWCCs of 140 Sicilian soils predicted by the AP model with α values formulated by the logistic growth equation were more biased than using α values given by the linear equation with regression coefficients directly from Arya et al. (1999). Therefore, the empirical parameters in the semi-physical models need to be determined in individual studies (Arya and Heitman, 2015; Jensen et al., 2015).

Attempts have been made to develop conceptual methods for reducing dependence on experimental data. Mohammadi and Vanclooster (2011) introduced a packing-state coefficient into the calculation of pressure heads for individual particle ranges in natural structure soil. The SWCCs predicted by this model (the MV model) approximated to the experimental SWCCs across 80 soils from the UNSODA hydraulic properties database (Mohammadi and Vanclooster, 2011). Arya and Heitman (2015) proposed a conceptual model (the AH model) involving only soil PSD and bulk density for predicting the SWCC. The predicted SWCCs showed reasonable to excellent agreement with experimental SWCCs in 75% of 41 soils from the UNSODA hydraulic properties database (Arya and Heitman, 2015). The performance of the conceptual procedures is generally robust and independent of soil type, allowing improvement of the SWCC prediction at regional or watershed scales.

The performance of semi-physical models could be affected by the database used for calibration and validation (Mohammadi and Vanclooster, 2011). The conceptual models have robust physical basis, but the reduced sensitivity to measured data might generate some deviations due to the simplified pore geometric concepts of the models, and the uncertainty and errors of measurements. Few studies comparing the semi-physical and conceptual models in SWCC prediction have been reported (Mohammadi and Vanclooster, 2011; Arya and Heitman, 2015). It is necessary to assess the applicability of these models in studies at regional or watershed scales in arid and semi-arid regions where the soil water content status is vital for plant growth. In the middle reaches of the Heihe River in northwestern China, various land use types intersperse with one another. Soils have a layered structure with obvious heterogeneity in both the horizontal and vertical directions (Li and Shao, 2013). It has been reported that land use, soil texture and structure have substantial effects on water retention (Hayashi et al., 2006; Wu et al., 2011; Haghverdi et al., 2015). Accurate prediction of soil water retention is essential for optimizing irrigation schedules, draining to alleviate salinization, and calculating ecological water requirement in this region.

The objectives of this study were: (1) to compare the performance of the AP, MV, and AH models, and Rosetta program in predicting the SWCC of various soil types, (2) to choose the most appropriate model for estimating AW in an oasis–desert transect in the middle reaches of the Heihe River basin.

2. Model description

2.1. Model theory

The idea of the three models (the AP model, MV model and AH model) emerges from the similarity between the shapes of the PSD and SWCC. The cumulative PSD is divided into m ($m \geqslant 20$) fractions, with solid mass and mean particle radius, w_i ($g\,g^{-1}$) and R_i (cm), respectively, for the ith fraction ($i = 1, 2, \cdots, m$). Solid particles in each fraction are assembled to form a hypothetical, cubic close-packed structure consisting of uniform-sized spherical particles with bulk density (ρ_b, $g\,cm^{-3}$) and particle density (ρ_s, $2.65\,g\,cm^{-3}$) equaling those measured on the natural structure sample.

The void ratio, e (dimensionless), is determined by:

$$e = (\rho_s - \rho_b)/\rho_b \tag{1}$$

Starting with the first fraction, calculated pore volumes are progressively summed and considered filled with water. The summation of filled pore volumes is divided by the bulk volume to obtain the volumetric water content, θ_i ($cm^3\,cm^{-3}$), which is given by (Arya and Paris, 1981):

$$\theta_i = \theta_s \sum_{j=1}^{j=i} W_j, \quad i = 1, 2, \cdots, m \tag{2}$$

where θ_s is the measured saturated water content ($cm^3\,cm^{-3}$).

Pressure heads, h_i (cm water), corresponding to pore radii are computed based on different hypotheses and explanations of the structure of each assemblage in these models. Brief introduction of the calculation of the three models are given sequentially in this study. Readers are referred to Arya et al. (1999), Mohammadi and Vanclooster (2011), and Arya and Heitman (2015) for detailed instructions on the AP, MV, and AH models, respectively.

2.2. Arya and Paris model

In this model, the pore volume formed by the assemblage with spherical particles in each fraction is approximated as a uniform-sized cylindrical capillary tube. The pore radius (r_i, cm) is related to R_i, and is calculated by (Arya and Paris, 1981):

$$r_i = 0.816 R_i \sqrt{e n_i^{(1-\alpha_i)}} \quad (3)$$

where n_i is the number of spherical particles for the i_{th} fraction and is given by (Arya and Paris, 1981):

$$n_i = 3W_i/(4\pi\rho_s R_i^3) \quad (4)$$

The variable α_i in Eq. (3) is the scaling parameter. Basile and D'Urso (1997) and Vaz et al. (2005) expressed α values as functions of h and θ, respectively. To decrease the uncertainty in the SWCC prediction caused by the interdependence of α on h or θ, we adopted the formulation proposed by Arya et al. (1999), that is,

$$\alpha_i = \log N_i / \log n_i \quad (5)$$

where N_i is the number of spherical particles required to trace the pore length for the i_{th} particle fraction in the natural structure soil.

According to Arya et al. (1999), N_i can be estimated from the measured PSD and experimental SWCC by:

$$N_i = 7.371 w_i e h_{mi}^2/(\rho_s R_i) \quad (6)$$

where h_{mi} is the pressure head on the measured SWCC.

A linear relationship between $\log N_i$ and $\log W_i/R_i^3$ is proposed by Arya et al. (1999) to obtain N_i more conveniently based on the linear dependence of n_i on W_i/R_i^3. This method is easy to use, and its performance is comparable with the logistic growth curve (Arya et al., 1999; Hwang and Powers, 2003; Soet and Stricker, 2003; Antinoro et al., 2014). Therefore, α_i is given by (Arya et al., 1999):

$$\alpha_i = [a + b\log(W_i/R_i^3)]/\log n_i \quad (7)$$

where a and b are unknown empirical parameters.

An equivalent pore radius is converted to h_i using the capillary equation (Arya and Paris, 1981):

$$h_i = \frac{2\gamma\cos\Theta}{\rho_w g r_i} = \frac{0.18}{R_i\sqrt{e n_i^{(1-a_i)}}} \quad (8)$$

where γ is the surface tension at the air–water interface (g s^{-2}), Θ is the contact angle (this model assumes perfect wettability, $\Theta = 0°$), ρ_w is the density of water (g cm^{-3}), g is the acceleration due to gravity (9.8 cm s^{-2}), and the number 0.18 represents a composite of constants. Readers are referred to Arya et al. (1999) for detailed instruction of the calculation.

2.3. Mohammadi and Vanclooster model

In the cubic, close packed assemblage with spherical particles assumed for each particle range, eight spherical particles are needed to form the narrowest region of an assembled pore. During the establishment of the SWCC from a drainage experiment on a saturated soil core, the pore water would drain from the pore when the metric suction head was larger than the air-entry value of the narrowest region of the assembled pore. The pore volume in an assemblage is needed intermediately to calculate the pressure head. The volume of a single assemblage yields $(4R_i)^3$, while the solid volume of eight spherical particles was $8(4\pi R_i^3)/3$. However, the number of spherical particles devoted to each assemblage could be less or more than eight in a natural structure. A coefficient

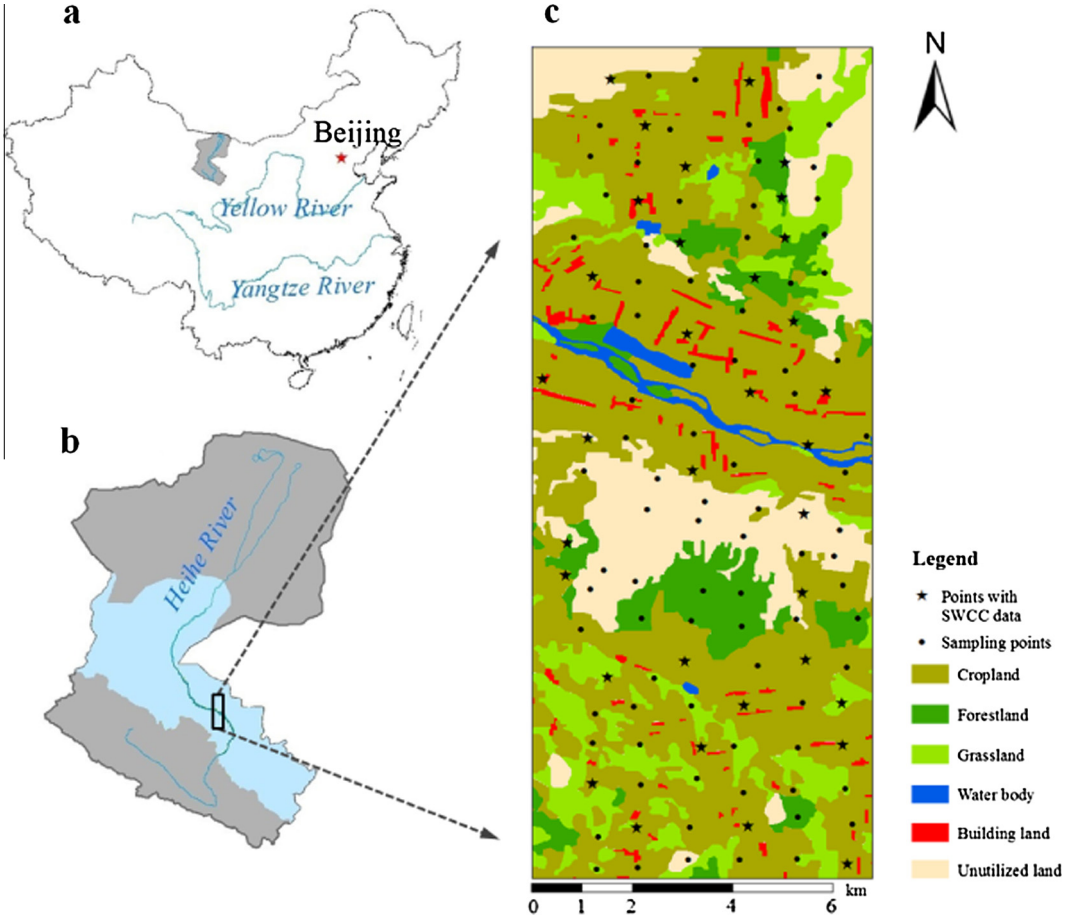

Fig. 1. The location of the sampling points (black circles) in the oasis-desert transect (c) in the middle reaches of the Heihe River basin (b) of China (a). The black five-pointed stars indicate the 34 representative points with measured soil water retention data points.

of packing states, ξ (dimensionless), is introduced (Mohammadi and Vanclooster, 2011):

$$\xi = \frac{6}{\pi(1+e)} \tag{9}$$

The h_i in a tube of general cross-sectional shape in the natural structure soil is thus given by (Tuller et al., 1999; Mohammadi and Vanclooster, 2011):

$$h_i = \xi \frac{C_{pi}}{A_{pi}} \frac{\gamma \cos \Theta}{\rho_w g} = \frac{1.038}{R_i(1+e)} \tag{10}$$

where C_{pi} (cm) and A_{pi} (cm^2) are the circumference ($2\pi R_i$) and area ($4R_i^2 - \pi R_i^2$) of the cross-section of the narrowest region of a single assembled pore, respectively, the meanings of γ, Θ, ρ_w, g, R_i, and e are the same as those aforementioned, and the number 1.308 represents a composite of constants. Readers for more detailed instruction are referred to Mohammadi and Vanclooster (2011).

2.4. Arya and Heitman model

For each particle fraction, corresponding to the cubic close-packed assemblage with spherical particles, the natural structure particles are also assumed to be packed in a cube. Focusing on one face of the cubes for the natural and hypothetical assemblages, assumptions are made: (1) pores in the two systems can be expressed as equivalent circular pores; and (2) the ratio of the pore sizes is proportional to the ratio of total pore areas on the face of the cubes for the two assemblages. For a given packing density and associated pore volume, longer pore length due to various lengths and jaggedness of particles in a natural assemblage means smaller radii and larger numbers of pores, both of which are related to particle numbers. A total of $n_i^{2/3}$ spherical particles are on one face of the cube for a closely-packed assemblage with spherical particles, contributing to a total length of $2R_i n_i^{2/3}$ by placing these particles end-to-end. However, the value of $2R_i n_i^{2/3}$ has to be adjusted within the length of the natural-structure cube in one dimension ($(w_i/\rho_b)^{1/3}$). By introducing the ratio $(w_i/\rho_b)^{1/3}/(2R_i n_i^{2/3})$ as the proportionality factor to account for the effects of deformation and packing density, the relationship between pore radii and pore areas can be rewritten as (Arya and Heitman, 2015):

$$\frac{\pi r_{in}^2}{\pi r_{ic}^2} = \frac{\phi (w_i/\rho_b)^{2/3}}{0.476(4n_i^{2/3}R_i^2)} \frac{(w_i/\rho_b)^{1/3}}{2R_i n_i^{2/3}} \tag{11}$$

where r_{in} and r_{ic} are the equivalent circular pore radius in the natural assemblage and close-packed assemblage with spherical particles, respectively, ϕ is the total porosity, equaling $1 - \frac{\rho_b}{\rho_s}$, and the number 0.476 is the porosity for spherical particles in the close-packed assemblage.

The cross-sectional area of a single pore for assemblage with spherical particles equals $(4-\pi)R_i^2$, so r_{in} is calculated, and the h_i for the natural structure soil is given by:

$$h_i = \frac{2\gamma \cos \Theta}{\rho_w g r_i} = \frac{0.180 w_i^{1/6}}{\sqrt{eR_i^3}} \tag{12}$$

where 0.180 is a composite of constants, and the variables γ, Θ, ρ_w, g, w_i, e, and R_i are the same aforementioned. Readers are referred to Arya and Heitman (2015) for detailed information of this model.

3. Materials and methods

3.1. Study area

The study was conducted in the middle reaches of the Heihe River basin, in Linze County of Gansu Province, China (Fig. 1). This region has a continental arid climate with a mean annual air temperate of 7.6 °C. The mean annual precipitation is 120 mm, approximately 60% of which occurs from July to September, and only 3% in winter. The mean annual potential evaporation is 2390 mm. The mean annual wind speed is 3.2 m s^{-1} and annual gale days (wind speed varies from 17.2 to 20.7 m s^{-1}) reach to 15 or more, and the sand-drifting mainly occurs from March to May.

A rectangular oasis–desert transect covering an area of 100 km^2 with a length of 20 km from north to south and a width of 5 km from east to west (39°12′30″–39°23′28″N, 100°05′32″–100°10′01″E, 1372–1417 m a.s.l.) was chosen for this study (Fig. 1b). The northern part of this transect includes the southern margin of the Badain Jaran Desert. The Heihe River flows across the area from east to west. This oasis–desert transect includes croplands with different cultivation histories, deserts with fixed and semi-fixed sand dunes, artificial grasslands in the oasis–desert ecotone, and natural grasslands in the bottomland. Main soil types include Aridisol derived from diluvial-alluvial materials in the northern marginal oasis, Entisols from the long-term encroachment and deposition of drift sand in the desert, Siltigi-Orhic Anthrosols after long-term cultivation in the old oasis, and Inceptisols in natural grassland according to the USDA Soil Taxonomy (Shirazi and Boersma, 1984; Li and Shao, 2014). The desert vegetation consists of *Halaxylon ammodendron* (C.A. Mey.) Bunge, *Calligonum mongolicum* Turcz., *Nitraria sphaerocarpa* Maxim and *Reaumuria soongorica* (Pall.) Maxim. The predominant grassland species are Common Reed (*Phragmites australis* (Cav.) Trin. ex Steud.), Common Leymus (*Leymus secalinus* (Georgi) Tzvel.), *Achnatherum splendens* (Trin.) Nevski, and *Kalidium foliatum* (Pall.) Moq. The main irrigated crops are maize (*Zea mays* L.) for grain, spring wheat (*Triticum aestivumLinn.*), tomatoes (*Solanum lycopersicum*) and sugar beets (*Beta vulgaris*) (Li and Shao, 2014).

3.2. Field sampling and laboratory analysis

A total 120 sampling points (56, 43 and 21 points for desert, cropland and grassland, respectively) were designed in the grid size of 1 × 1 km throughout the area except where was unreachable (Fig. 1c). Thirty-four of the 120 points were selected as representative of desert, cropland and grassland with 15, 12 and 7 points, respectively (Fig. 1c). At each of these representative points, disturbed soil samples were collected using a 5 cm diameter hand auger at a depth interval of 20 cm within a 1 m profile. Soil sample for each layer was taken with three duplicates randomly collected at a 5 × 5 m plot at each point. A profile was dug to 1.0 m depth, and one undisturbed soil core was collected in each layer at 20 cm depth intervals using stainless-steel cutting rings (5.0 cm in height by 5.0 cm in diameter). The sampling was conducted in April 2011, and all disturbed soil samples and undisturbed soil cores were well preserved and taken to the laboratory.

In the laboratory, disturbed soil samples were air dried and passed through a 2 mm mesh after removing the organic debris. The soil PSD was measured by laser diffraction using a Mastersizer 2000 analyzer (Malvern Instruments, Malven, England). Arya and Paris (1981) suggested $m = 20$ as a least number of fractions. The soil PSD was classified into 20 fractions with boundaries at particle diameters of 1, 2, 7, 8, 10, 20, 30, 40, 50, 60, 70, 80, 100, 150, 200, 250, 400, 500, 800, and 2000 μm during the measurement in this study. Measured soil textures covered eight classes including silt

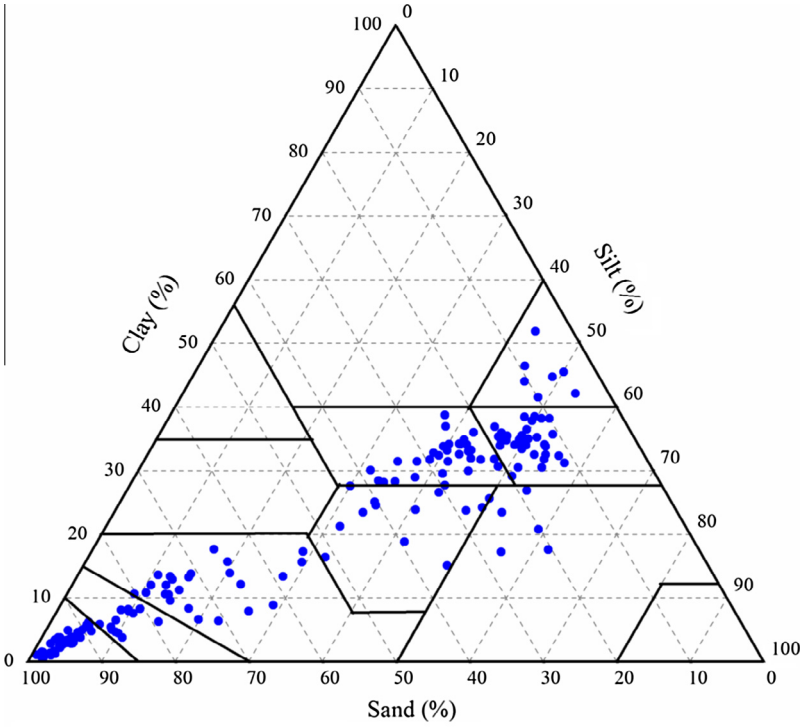

Fig. 2. Textural distribution of the 170 soil samples at the 34 representative points according to the USDA Soil Taxonomy.

loam, silty clay loam, silty clay, loam, clay loam, sandy loam, loamy sand, and sand according to the USDA Soil Taxonomy (Fig. 2) (Shirazi and Boersma, 1984).

The undisturbed soil core was saturated from below, and its saturated weight was measured. The saturated soil core was used to measure the SWCC data points using a high speed centrifuge (Nimmo et al., 2002). The saturated soil core was placed into the centrifuge bucket, and then fixed in the centrifuge rotor by guaranteeing the balance of weights of the four buckets in the rotor. The centrifuge was run by setting centrifuge speeds and time to reach the given h values. The weight of the core was measured when the thirteen set h values of −10.2, −51.0, −102.0, −204.0, −408.1, −612.1, −816.1, −1020.2, −2040.3, −4080.6, −6121.0, −8161.3, and −10201.6 cm of water were reached after centrifuging for 10, 17, 26, 36, 45, 51, 55, 58, 68, 77, 83, 87, and 90 min, respectively. The final soil core was oven dried at 105 °C for 48 h after removing the bucket. The dry weight of solid mass was measured to determine the bulk density, which was used to convert the mass water content into volumetric water content under each h. To obtain the continuous SWCC, the van Genuchten equation was used to fit experimental data (van Genuchten, 1980). An iterative non-linear regression procedure was employed to find the values of the fitting parameters in van Genuchten equation that give the most approximation between experimental and predicted data. This fitting procedure was performed using the RETC program (van Genuchten et al., 1991).

3.3. Evaluation of models

The soil-specific empirical parameter, α_i, in the AP model need to be determined first when calculating the pressure head corresponding to each particle range. Furthermore, the application of the three models has to be adapted to the considered situation in this study. Therefore, the 170 samples with SWCC data at representative points were randomly split into a calibration dataset (n = 92) for determining the values of a and b, in turn, the α_i value of the AP model, and a validation dataset (n = 78) for evaluating the predictive accuracy of the three models. The numbers of samples for each of the textural classes in the two datasets were proportional to their occurrence in the total dataset (Table 1).

In the validation dataset, the calculated SWCC data points for the AP, MV and AH models can be obtained by pairing θ_i in Eq. (2) with h_i in Eqs. (8), (10) and (12), respectively. The van Genuchten equation was adopted to obtain the SWCC after having fitted the parameters using the RETC program based on the 20 water retention data points for each sample predicted by the model (van Genuchten et al., 1991). On these predicted curves, the θ values corresponding to the thirteen actual measured h values (−10.2, −51.0, −102.0, −204.0, −408.1, −612.1, −816.1, −1020.2, −2040.3, −4080.6, −6121.0, −8161.3, and −10201.6 cm of water) can be determined and was compared with the measured θ values. The soil water contents at field capacity and wilting point were obtained from the calculated SWCC. Compared to the attainment of field capacity under a prescribed uniform matric potential value, Assouline and Or (2014) proposed a new static criteria to determine the specific pressure heads at field capacity for different soil types. Water retentions at h of −100 and −330 cm of water were

Table 1
The soil texture and sample number in the calibration and validation datasets.

Soil texture	Total number	Number for calibration	Number for validation
Silt loam	10	5	5
Silty clay loam	28	16	12
Silty clay	9	5	4
Loam	11	6	5
Clay loam	30	20	10
Sandy loam	10	5	5
Loamy sand	18	9	9
Sand	54	26	28
Total	170	92	78

commonly considered as field capacity for coarse- and fine-textured soils, respectively (Rivers and Shipp, 1972; Gijsman et al., 2003; Haghverdi et al., 2015). Therefore, water content at field capacity was set at h of −330 cm of water for the first six textural classes and −100 cm of water for loamy sand and sand soils in this study. Water content at h of −15000 cm of water was chosen as wilting point for all textural classes. The AW predicted by the models was estimated for each sample in the validation dataset. The calculated AW values were compared with those derived from the experimental SWCCs. When no measurement has been done, the soil water contents at field capacity and wilting point can be conveniently derived from the van Genuchten equation of SWCC (van Genuchten, 1980) after having determined the parameters using the Rosetta program (Botula et al., 2012). To further validate the predictive accuracy of the three models, the predicted AW values were also compared with those from the Rosetta program using sand/silt/clay contents and bulk density as input variables.

Three statistical criteria were used to measure the performance of the models in predicting both θ on the SWCC and AW, including the coefficient of determination (R^2), the mean error (ME, cm^3 - cm^{-3}), and the root mean square error (RMSE, $cm^3\,cm^{-3}$), which are given by:

$$R^2 = \left[\frac{\sum_{i=1}^{n}(O_i-\overline{O})(P_i-\overline{P})}{\left[\sum_{i=1}^{n}(O_i-\overline{O})^2\right]^{0.5}\left[\sum_{i=1}^{n}(P_i-\overline{P})^2\right]^{0.5}}\right]^2 \quad (13)$$

$$\mathrm{ME} = \frac{1}{n}\sum_{i=1}^{n}(P_i-O_i) \quad (14)$$

$$\mathrm{RMSE} = \sqrt{\frac{\sum_{i=1}^{n}(P_i-O_i)^2}{n}} \quad (15)$$

where O_i and P_i are the measured and predicted values, respectively, $\overline{O}$ and $\overline{P}$ are the averages of measured and predicted values, respectively, and n is the number of observations in the validation dataset. The R^2 values range from 0 to 1, and RMSE values are not less than zero. The model with the highest predictive accuracy was regarded as the one with the highest R^2 value, the lowest absolute value of ME, and the lowest RMSE value.

4. Results and discussion

4.1. Predictive accuracy of the three models for SWCC

The value of N_i corresponding to each particle range of each sample was calculated according to Eq. (6). The values decreased gradually from fine to coarse particle fractions, and differed among textural classes for the same particle range. The linear relationship between $LogN_i$ and $Log(W_i/R_i^3)$ in the AP model was well fitted for each of the eight textural classes in the calibration dataset, with R^2 values ranging from 0.836 for sand to 0.959 for silty clay (Fig. 3). The coefficients of a and b were determined as the intercept and slope of the linear regression equation, respectively, for each of the eight textural classes (Fig. 3). The coefficient a differed greatly, while the b values varied slightly, among different textural classes. The α_i value for each particle range of samples in the calibration and validation datasets was calculated using a and b values for each textural class in Fig. 3 according to Eq. (7).

Fig. 4 shows a comparison of the predicted θ values by the AP, MV and AH models, and Rosetta program with the experimental θ values under the thirteen actual measured h values for the samples in the validation dataset. The use of θ instead of h was to prevent possible biases in the optimized α_i value due to the use of log-transformed h values. This procedure is of more practical interest to assess the accuracy of a prediction model as it relates directly to the water mass balance of the soil profile (Antinoro et al., 2014). Pairs of the predicted and measured θ values for all textural classes were pooled.

For the AP model, visual inspection indicates that the majority of the points were concentrated around the 1:1 line (Fig. 4a). An overall good agreement was observed between the predicted and measured θ values, since the linear regression had an R^2 value of 0.863, and both the ME (−0.008 $cm^3\,cm^{-3}$) and RMSE (0.049 cm^3 - cm^{-3}) were close to zero. The linearly fitted α_i values, however, overestimated the experimental θ values under h between −10.20 and −204.03 cm of water for sand soil where the data points remarkably deviated from the 1:1 line (Fig. 4a). After removing these data points, the predicted θ values approximated to the experimental values, with R^2 of 0.932, the ME and RMSE of −0.015 and 0.037 $cm^3\,cm^{-3}$, respectively. This result indicates that

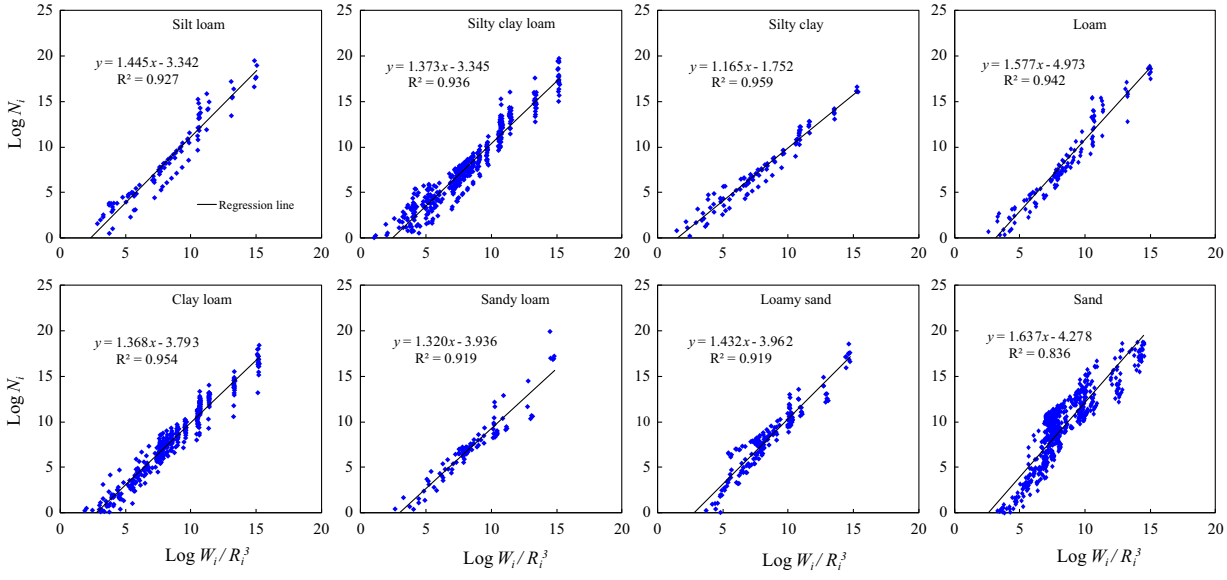

Fig. 3. Relationship between the number of spherical particles to trace the pore lengths in natural structure soil (log N_i) and the ratio of solid mass fraction to mean particle diameter (log W_i/R_i^3) for all textural classes in the calibration dataset.

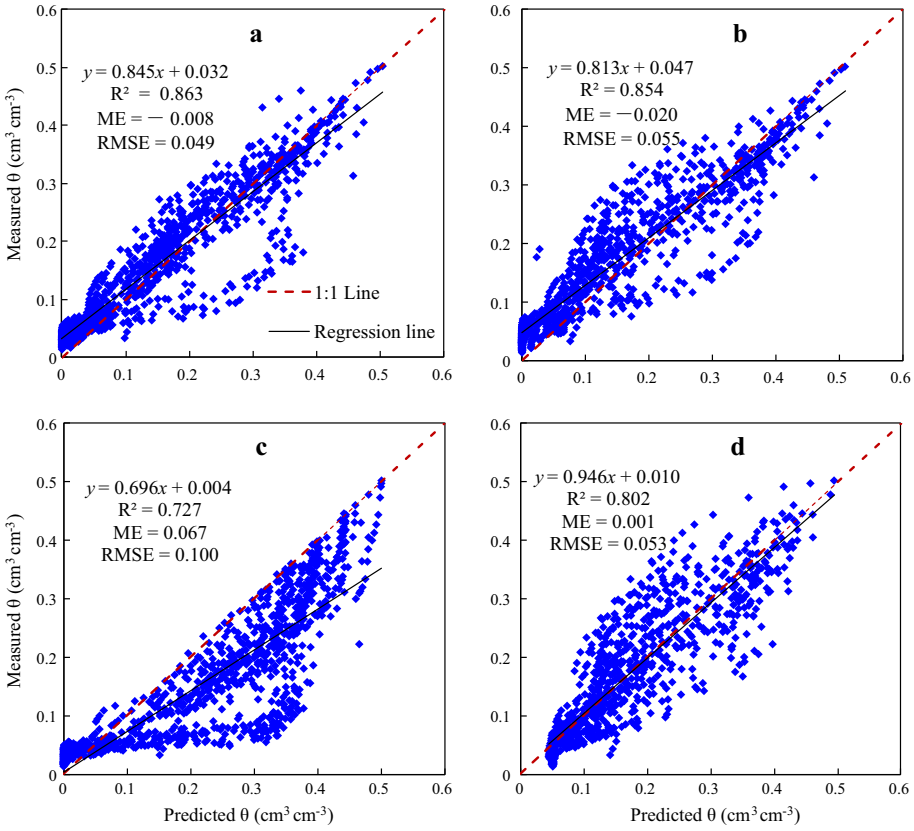

Fig. 4. Comparison of the measured and predicted soil water content by the (a) AP model, (b) MV model, (c) AH model and (d) Rosetta program for samples in the validation dataset. The soil water contents were under the actual measured pressure heads on the soil water characteristic curves.

Table 2
Summary statistics of the measured and predicted field capacity, wilting point, and available water content by the AP model, MV model, and Rosetta program for the eight textural classes in the validation dataset.

Property[a]	Method	Silt loam	Silty clay loam	Silty clay	Loam	Clay loam	Sandy loam	Loamy sand	Sand
Fc ($cm^3\ cm^{-3}$)	Measured	0.37 ± 0.01[b]	0.33 ± 0.05	0.36 ± 0.07	0.25 ± 0.05	0.24 ± 0.04	0.16 ± 0.02	0.13 ± 0.03	0.10 ± 0.02
	AP	0.38 ± 0.01	0.34 ± 0.04	0.36 ± 0.05	0.22 ± 0.05	0.21 ± 0.04	0.10 ± 0.01	0.11 ± 0.01	0.14 ± 0.04
	MV	0.30 ± 0.03	0.33 ± 0.03	0.36 ± 0.05	0.21 ± 0.04	0.23 ± 0.04	0.14 ± 0.01	0.15 ± 0.01	0.09 ± 0.04
	Rosetta	0.27 ± 0.02	0.28 ± 0.02	0.30 ± 0.01	0.23 ± 0.01	0.25 ± 0.01	0.19 ± 0.01	0.21 ± 0.02	0.09 ± 0.02
Wp ($cm^3\ cm^{-3}$)	Measured	0.18 ± 0.02	0.19 ± 0.03	0.18 ± 0.02	0.12 ± 0.03	0.12 ± 0.04	0.07 ± 0.02	0.04 ± 0.02	0.02 ± 0.01
	AP	0.12 ± 0.03	0.15 ± 0.01	0.16 ± 0.01	0.11 ± 0.02	0.11 ± 0.01	0.05 ± 0.01	0.05 ± 0.01	0.01 ± 0.01
	MV	0.08 ± 0.01	0.11 ± 0.02	0.13 ± 0.01	0.06 ± 0.01	0.08 ± 0.01	0.05 ± 0.01	0.05 ± 0.01	0.01 ± 0.01
	Rosetta	0.09 ± 0.01	0.12 ± 0.01	0.15 ± 0.01	0.10 ± 0.01	0.12 ± 0.01	0.08 ± 0.02	0.06 ± 0.01	0.05 ± 0.01
AW ($cm^3\ cm^{-3}$)	Measured	0.19 ± 0.01	0.15 ± 0.03	0.18 ± 0.05	0.13 ± 0.02	0.12 ± 0.02	0.09 ± 0.01	0.09 ± 0.02	0.09 ± 0.02
	AP	0.26 ± 0.03	0.19 ± 0.04	0.20 ± 0.04	0.10 ± 0.04	0.10 ± 0.03	0.05 ± 0.01	0.06 ± 0.01	0.13 ± 0.04
	MV	0.22 ± 0.02	0.22 ± 0.03	0.23 ± 0.05	0.15 ± 0.05	0.14 ± 0.03	0.09 ± 0.01	0.10 ± 0.01	0.09 ± 0.04
	Rosetta	0.18 ± 0.02	0.16 ± 0.02	0.15 ± 0.01	0.12 ± 0.01	0.13 ± 0.02	0.10 ± 0.02	0.15 ± 0.02	0.04 ± 0.03

[a] Fc, Wp and AW refer to field capacity, wilting point, and available water content, respectively.
[b] Mean ± one standard deviation.

the AP model did worse in predicting water retention under lower pressure heads (h ranges from −10.20 and −204.03 cm of water) for a majority of sand soil.

The MV model generally predicted water retention well, with an R^2 value of 0.854, and ME and RMSE values of −0.020 and 0.055 $cm^3\ cm^{-3}$, respectively (Fig. 4b). The MV model also somewhat overestimated soil water retention under h ranging from −10.20 to −51.01 cm of water for a few sand soil samples. The deviation, however, was smaller than that of the AP model. The linear fitting between experimental and predicted θ values also improved after eliminating these data points (R^2 = 0.896, ME = −0.025 $cm^3\ cm^{-3}$, RMSE = 0.050 $cm^3\ cm^{-3}$). Both the ME values for the AP and MV models, with and without the largely deviated data points of sand soil, were negative, indicating that these two models overall slightly underestimated experimental θ values, although their performances were generally acceptable and evenly matched.

For the AH model, almost all the predicted θ values were larger than the measured values, since almost all of the data points were located below the 1:1 line (Fig. 4c). The R^2 (0.727) was the smallest, and the absolute values of ME (0.067 $cm^3\ cm^{-3}$) and RMSE (0.100 $cm^3\ cm^{-3}$) were the largest among the three models (Fig. 4a–c). This result indicates that the AH model tended to overestimate the experimental θ in the full range of the SWCC. The predicted θ values by the Rosetta program was well fitted to the experimental values with the highest slope and the lower intercept

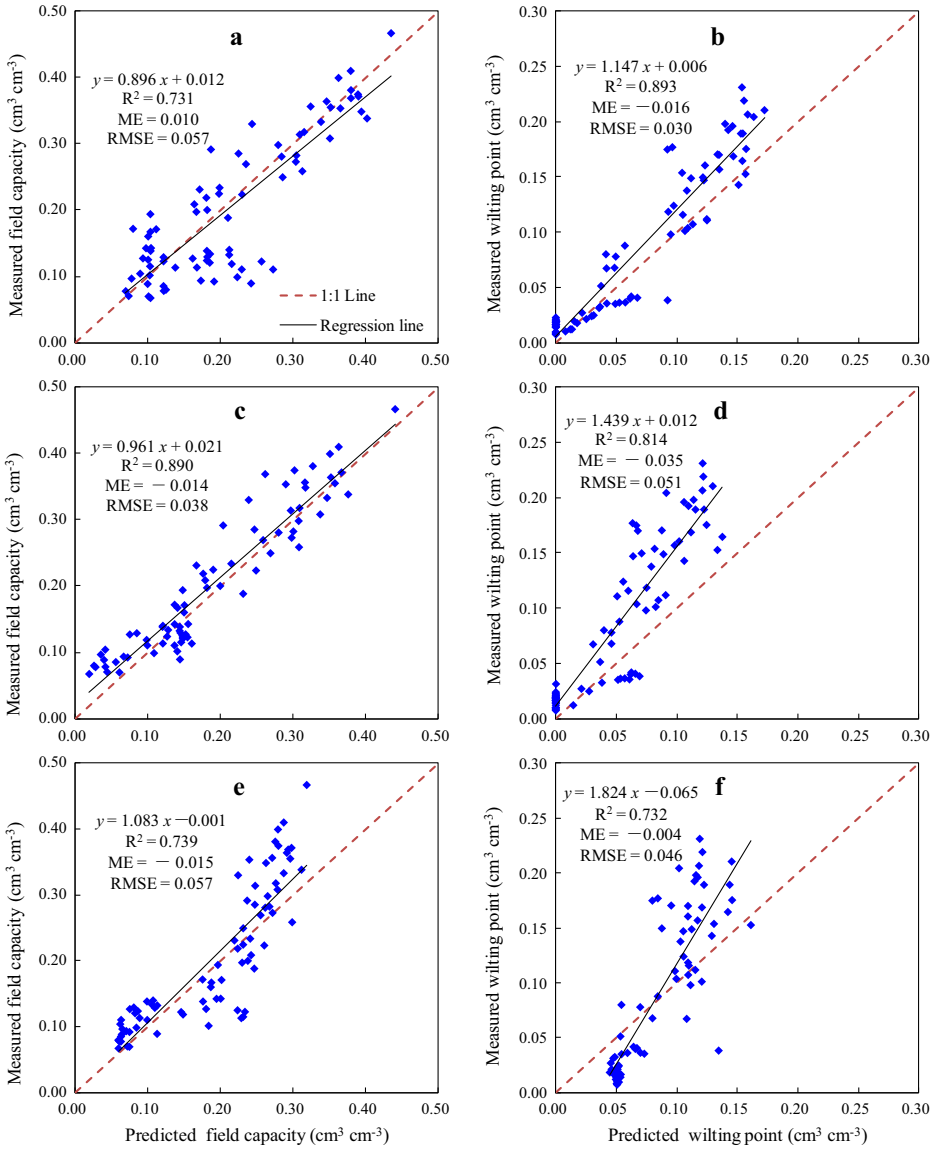

Fig. 5. Comparison of the measured and calculated soil water contents at field capacity and wilting point predicted by the (a and b) AP model, (c and d) MV model, and (e and f) Rosetta program for the eight textural classes in the validation dataset. The left column refers to field capacity under pressure heads of −330 cm of water for the first six textural classes and −100 cm of water for loamy sand and sand soils. The right column refers to wilting point under pressure head of −15,000 cm of water.

values (Fig. 4d). The R^2, ME and RMSE for Rosetta program were 0.802, 0.001 $cm^3\ cm^{-3}$ and 0.053 $cm^3\ cm^{-3}$, respectively. The regression line nearly overlapped the 1:1 line without obvious deviation in any range of the SWCC (Fig. 4d).

The slight overprediction in the wet range and slight underprediction in the dry range of the SWCC were common for the AP and MV models (Fig. 4). This bias has been reported by Arya et al. (1999) and Antinoro et al. (2014) for the AP model, and by Mohammadi and Vanclooster (2011) for the MV model. The models assumed that the particle size and the bulk density are primary determinants of pore size. In natural soils, aggregation of primary particles into secondary and tertiary particles, the geometric features of root channels, microscopic cracks, and wormholes are not fully represented by the PSD and bulk density (Arya and Paris, 1981; Or and Tuller, 1999; Hwang and Powers, 2003). The relative abundance of such pores affects the extent to which the predictions would deviate from measurements. In the wet range, the SWCC is governed by capillary forces, the presence of structural cracks or macropores, and structural disturbances during the sampling and handling may result in lower measured than predicted θ values (Arya and Paris, 1981; Antinoro et al., 2014). In the dry range of the SWCC, water is dominated by adsorptive forces (Or and Tuller, 1999; Jensen et al., 2015). The incomplete desorption

Table 3
The mean relative error ($\overline{RE}$, %) between the predicted available water contents by the AP model, MV model, Rosetta program, and the experimental available water contents for soils in the validation dataset.

Texture	AP model	MV model	Rosetta
Silt loam	36.9	18.0	8.6
Silty clay loam	32.9	48.6	20.9
Silty clay	15.3	28.2	21.6
Loam	26.4	8.5	11.6
Clay loam	22.4	26.7	24.6
Sandy loam	43.2	14.3	25.5
Loamy sand	37.4	11.8	50.9
Sand	56.0	31.6	62.4
Total	39.8	27.4	38.7

The mean relative error is calculated as: $\overline{RE} = \frac{1}{n}\sum_{i=1}^{n}\frac{|O_i - P_i|}{O_i} \times 100\%$, where O_i and P_i refer to the observed and predicted values, respectively.

of residual water held as films or in dead-end soil pores would lead to higher experimental than predicted θ values, since the models assumed complete desorption of given-size pores when the corresponding capillary pressure was applied (Or and Tuller, 1999; Mohammadi and Vanclooster, 2011; Antinoro et al., 2014). Additionally, the packing parameter ξ does not fully reflect the pore geometry, which may also contribute to the MV model error (Mohammadi and Vanclooster, 2011).

Many factors not fully explained by the three models contribute to the deviation of the predictions from the experimental data. Non-linearity between PSD and pore size distribution, complex pore geometry, hysteresis, volume change of clay fraction upon wetting and drying, and uncertainties in the measurements will all contribute to the observed disparities (Arya and Paris, 1981; Rouault and Assouline, 1998; Hwang and Powers, 2003). Additionally, the three models assumed water retention within pores by capillary action, which was not always true. Except for the distinction of dominant forces for water retention in the dry and wet ranges of the SWCC, clay particles retain water primarily by surface sorption (Hwang and Powers, 2003; Hwang and Choi, 2006). Therefore, the models might be more suitable for rigid soils with medium grain size than fine-textured soils.

In summary, the AP and MV models, and Rosetta program outperformed the AH model in predicting the SWCC in this study. A closer agreement between the prediction of the AP model and the experimental data should be expected, since its empirical parameters were derived from the measured SWCC data. The Rosetta program was developed based on three databases containing a large number of soil hydraulic data and predictive soil properties (Schaap et al., 2001). The feasibility of the Rosetta program results was therefore taken for granted once the input data were determined. However, the MV model are more attractive for practical applications at catchment or regional scales because they are no longer dependent on soil empirical and database-related parameters.

4.2. Prediction of field capacity and wilting point

Filed capacity and wilting point on the experimental SWCCs decreased from fine- to coarse-textured soils in the validation dataset (Table 2). Weak spatial variability in field capacity was observed for silt loam because the coefficients of variation (CVs = 0.04) were not larger than the threshold value of 0.10 (Nielsen and Bouma, 1985). The CVs ranging from 0.14 to 0.22 indicated moderate spatial variability in field capacity for other textural classes. Moderate spatial variability of wilting point were observed for the eight textural classes because the CV varied from 0.11 for silt loam to 0.37 for sand soil (Nielsen and Bouma, 1985) (Table 2).

Field capacity and wilting point on the SWCCs predicted by the AP and MV models and Rosetta program were compared with the experimental values (Fig. 5). The MV model performed better than the AP model and Rosetta program in predicting field capacity. The AP model slightly overestimated the measured field capacity due to the influence of some sand soils with relatively higher field capacity values (Fig. 5a). The MV model and Rosetta program overall underestimated experimental field capacity data (Fig. 5c and e). On the other hand, the AP model did better than the MV model and Rosetta program in predicting wilting point. All the three methods overall underestimated experimental wilting point because of the negative ME values (Fig. 5b, d and f). The CVs for field capacity and wilting point of sand soil predicted by the AP and MV models were larger than those for other textural classes. The spatial variability for wilting point of sand predicted by the AP (CV = 1.55) and MV (CV = 3.18) models was strong (Table 2). However, field capacity and wilting point predicted by Rosetta program showed weak spatial variability, except field capacity for sand (CV = 0.29) and wilting point for sandy loam (CV = 0.18) (Table 2).

4.3. Estimation of available water content

The AW values were determined for the AP and MV models, Rosetta program, and experimental data for each sample in the validation dataset. The mean AW values calculated by the AP and MV models were higher than the measured values for the silt loam, silty clay loam, and silty clay soils. The mean AW values predicted by the MV model for the remaining five textural classes and those by the Rosetta program for the first six textural classes approximated to the measured AW values (Table 2). This could also be

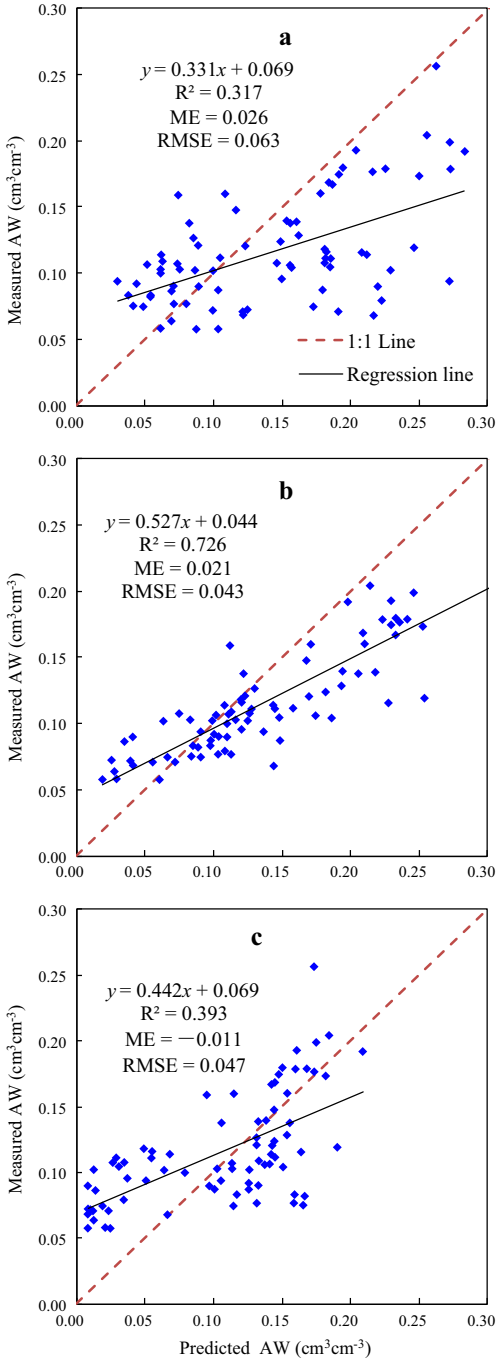

Fig. 6. Comparison of the measured and predicted available water content (AW) by the (a) AP model, (b) MV model, and (c) Rosetta program for soils in the validation dataset.

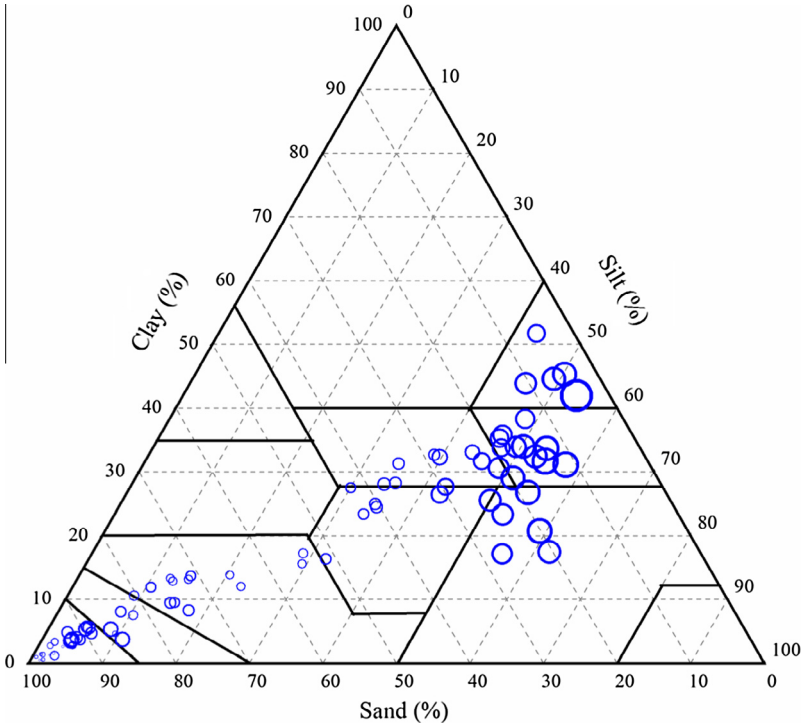

Fig. 7. Distribution of available water content predicted by the MV model for samples in the validation dataset. The circle size refers to the magnitude of AW values. The larger the circle, the higher the AW value, and vice versa.

reflected by the values of mean relative error listed in Table 3. The mean AW values derived from the AP model and Rosetta program for loamy sand and sand deviated much from those predicted by the MV model and the experimental values (Table 2). The mean relative errors of the AP model and Rosetta program for these two textural classes were much higher than that of the MV model (Table 3). The AW values for the AP and MV models and experimental data exhibited moderate spatial variability for the textural classes, except silt loam which had weak spatial variability (CV = 0.10, 0.08 and 0.06, respectively) (Table 2). The AW values predicted by the Rosetta program showed weak spatial variability for the first four textural classes and moderate variability for the remaining classes (Table 2). Compared with the Rosetta program, the AP and MV models predicted higher AW values for silt loam, silty clay loam, silty clay, and sand soils (Table 2). It shows that field capacity, wilting point and the AW vary greatly, not only among methods and textural classes, but also within soil types (e.g., sand soil).

Fig. 6 shows the goodness-of-fit between the predicted and experimental AW values by pooling the textural classes. In general, a majority of the predicted AW values by the AP and MV models were greater than the experimental ones (Fig. 6a and b). The Rosetta program predicted AW values lower than the experimental values (Fig. 6c). Overall, the MV model predicted relatively accurate AW values with higher R^2, lower RMSE and lower mean relative error (Fig. 6, Table 3). However, the R^2 value (0.726) was more modest than that for soil water content (0.854, Fig. 4b) and field capacity (0.890, Fig. 5c). The underestimation of field capacity for sand soil (Fig. 5c) and wilting point for silty clay loam soil (Fig. 5d) contributed to the deviation of the AW values of the MV model from the experimental ones (Table 3, Fig. 6).

The MV model generally performed well in indirectly predicting AW for all textural classes in this study. This highlights the advantages of the MV model of having robust physical basis and being independent of measured data over the AP model. On the other hand, the MV model predicts water retention by involving precise subclasses of texture data rather than simply basing on broadly-defined soil type like the practice of Rosetta. The AW values predicted by the MV model for samples in the validation dataset are shown in the ternary diagrams (Fig. 7). The size of the circles corresponded to the magnitude of the AW values. The larger the circle, the higher the AW value, and vice versa (Fig. 7). The larger AW values were for fine-textured soils, while the coarse textured classes of sandy loam, loamy sand, and sand showed lower AW values (Fig. 7). This reflects the positive correlation between water retention and fine particle content. The clay fraction favors the occurrence of micropores, which generate capillary forces. High clay content can also increase the specific surface area of the soil matrix, and enhance water adsorption (Botula et al., 2012). Haghverdi et al. (2015) reported that a reduction in AW was consistent with an increase in sand content with increasing soil depth. However, the AW values for silty clay, silty clay loam and silt loam approximated to each other. This is consistent with the report that soils with a high clay fraction showed a high proportion of water unavailable for plants (Al Majou et al., 2008; Ramos et al., 2014).

It is noteworthy that the MV model have not sufficiently taken into account soil structure, which is an important factor determining a soil's capacity to retain water (Gijsman et al., 2003; Pachepsky and Rawls, 2003). Field-measured data on the critical volumetric water contents may be need to improve the models' accuracy by incorporating the effects of soil structure on water retention (Pachepsky and Rawls, 2003). On the other hand, the AW is merely the "capacity" of soil water available for plants. A high AW does not necessarily mean the plant has easy access to the water, because the water uptake capability of roots is a function of wilting point. A higher wilting point means a lower water uptake at a certain soil–water content (Gijsman et al., 2003). For water management, the actual available water content, its spatial distribution and temporal variability are more important (Haghverdi et al., 2015). Therefore, we will focus on analyzing

the actual available water content in root zone and its variation during the growing season, aiming to explore its relationship with plant growth and to improve water use efficiency in future studies.

5. Conclusions

In this study, we compared the performance of the semi-physical AP model, conceptual MV and AH models, and Rosetta program in predicting the SWCC and AW from the soil particle-size distribution and bulk density at 34 points representing different landscapes in an oasis–desert transect in the middle reaches of the Heihe River basin, northwestern China. Two unknown empirical parameters, for deriving the scaling parameter by the linear equation, of the AP model were determined for each textural class using 92 soil samples covering eight textural classes in the calibration dataset. The AP model, MV model and Rosetta program showed better agreement with the experimental SWCCs than the AH model for 78 samples in the validation dataset. Different degrees of spatial variability in filed capacity, wilting point and AW were observed among the methods and textural classes. Great variations in the three properties also existed within textural class, especially sand soil. Therefore, the semi-physical and conceptual models may be more promise by having robust physical basis and involving specified subclasses of texture data than the Rosetta program, which is based on neural network analysis and acts on broadly-defined soil types. Furthermore, the MV model is not prone to the uncertainty and errors of measurements because it is independent of experimental data, while the practices of the AP model and Rosetta program are database dependent. The MV model outperformed the AP model and Rosetta program in predicting AW. The results of this study indicate that the MV model is useful for improving soil water retention prediction at regional or watershed scales, which then benefits the application of hydrological models and soil water management in arid regions.

Acknowledgements

This study was finally supported by the National Natural Science Foundation of China (91425301 and 91025018). We appreciate the help for laboratory analysis from the staff of the State Key Laboratory of Soil Erosion and Dryland Farming on the Loess Plateau, Institute of Soil and Water Conservation, Chinese Academy of Sciences. The authors sincerely thank the three anonymous reviewers for their constructive comments, which helped us greatly to improve the quality of this manuscript.

References

Al Majou, H., Bruand, A., Duval, O., Le Bas, C., Vautier, A., 2008. Prediction of soil water retention properties after stratification by combining texture, bulk density and the type of horizon. Soil Use Manage. 24 (4), 383–391.

Antinoro, C., Bagarello, V., Ferro, V., Giordano, G., Iovino, M., 2014. A simplified approach to estimate water retention for Sicilian soils by the Arya–Paris model. Geoderma 213, 226–234.

Arya, L.M., Bowman, D.C., Thapa, B.B., Cassel, D.K., 2008. Scaling soil water characteristics of golf course and athletic field sands from particle-size distribution. Soil Sci. Soc. Am. J. 72 (1), 25–32.

Arya, L.M., Heitman, J.L., 2015. A non-empirical method for computing pore radii and soil water characteristics from particle-size distribution. Soil Sci. Soc. Am. J. http://dx.doi.org/10.2136/sssaj2015.04.0145.

Arya, L.M., Leij, F.J., van Genuchten, M.Th., Shouse, P.J., 1999. Scaling parameter to predict the soil water characteristic from particle-size distribution data. Soil Sci. Soc. Am. J. 63 (3), 510–519.

Arya, L.M., Paris, J.F., 1981. A physicoempirical model to predict the soil moisture characteristic from particle-size distribution and bulk density data. Soil Sci. Soc. Am. J. 45 (6), 1023–1030.

Assouline, S., Or, D., 2014. The concept of field capacity revisited: defining intrinsic static and dynamic criteria for soil internal drainage dynamics. Water Resour. Res. 50, 4787–4802.

Basile, A., D'Urso, G., 1997. Experimental correlations of simplified methods for predicting water retention curves in clay-loamy soils form particle-size determination. Soil Technol. 10 (3), 261–272.

Bayat, H., Neyshaburi, M.R., Mohammadi, K., Nariman-Zadeh, N., Irannejad, M., Gregory, A.S., 2013. Combination of artificial neural networks and fractal theory to predict soil water retention curve. Comput. Electron. Agric. 92, 92–103.

Botula, Y.D., Cornelis, W.M., Baert, G., Van Ranst, E., 2012. Evaluation of pedotransfer functions for predicting water retention of soils in Lower Congo (D.R. Congo). Agric. Water Manage. 111, 1–10.

Ghanbarian, B., Taslimitehrani, V., Dong, G.Z., Pachepsky, Y.A., 2015. Sample dimensions effect on prediction of soil water retention curve and saturated hydraulic conductivity. J. Hydrol. 528, 127–137.

Gijsman, A.J., Jagtap, S.S., Jones, J.W., 2003. Wading though a swap of complete confusion: how to choose a method for estimating soil water retention parameters for crop models. Eur. J. Agron. 18, 77–106.

Haghverdi, A., Leib, B.G., Washington-Allen, R.A., Ayers, P.D., Buschermohle, M.J., 2015. High-resolution prediction of soil available water content within the crop root zone. J. Hydrol. 530, 167–179.

Hayashi, Y., Ken'ichirou, K., Mizuyama, T., 2006. Changes in pore size distribution and hydraulic properties of forest soil resulting from structural development. J. Hydrol. 331 (1–2), 85–102.

Hosseini, F., Mosaddeghi, M.R., Hajabbasi, M.A., Sabzalian, M.R., 2016. Role of fungal endophyte of tall fescue (Epichloë coenophiala) on water availability, wilting point and integral energy in texturally-different soils. Agric. Water Manage. 163, 197–211.

Hwang, S.Il., Choi, S.Il., 2006. Use of a lognormal distribution model for estimating soil water retention curves from particle-size distribution data. J. Hydrol. 323 (1–4), 325–334.

Hwang, S.Il., Powers, S.E., 2003. Using particle-size distribution models to estimate soil hydraulic properties. Soil Sci. Soc. Am. J. 67 (4), 1103–1112.

Jensen, D.K., Tuller, M., de Jonge, L.W., Arthur, E., Moldrup, P., 2015. A new two-stage approach to predicting the soil water characteristic from saturation to oven-dryness. J. Hydrol. 521, 498–507.

Lawes, R.A., Oliver, Y.M., Robertson, M.J., 2009. Integrating the effects of climate and plant available water holding capacity on wheat yield. Field Crops Res. 113 (3), 297–305.

Leij, F.J., Alves, W.J., van Genuchten, M.Th., Williams, J.R., 1996. The UNSODA Unsaturated Soil Hydraulic Database. User's Manual Version 1.0. National Risk Management Research Laboratory, Office of Research and Development, US Environmental Protection Agency, 103.

Li, D.F., Shao, M.A., 2013. Simulating the vertical transition of soil textural layers in north-western China with a Markov chain model. Soil Res. 51 (3), 182–192.

Li, D.F., Shao, M.A., 2014. Soil organic carbon and influencing factors in different landscapes in an arid region of northwestern China. Catena 116, 95–104.

Mohammadi, M.H., Vanclooster, M., 2011. Predicting the soil moisture characteristic curve from particle size distribution with a simple conceptual model. Vadose Zone J. 10 (2), 594–602.

Nemes, A., Rawls, W.J., 2006. Evaluation of different representations of the particle-size distribution to predict soil water retention. Geoderma 132 (1–2), 47–58.

Nemes, A., Rawls, W.J., Pachepsky, Y.A., 2006. Use of the nonparametric nearest neighbor approach to estimate soil hydraulic properties. Soil Sci. Soc. Am. J. 70 (2), 327–336.

Nielsen, D.R., Bouma, J., 1985. Soil spatial variability. In: Proceedings of Workshop of the ISSS and the SSSA. 30 November–1 December 1984, Las Vegas, NV. Pudoc, Wageningen, The Netherlands.

Nimmo, J.R., Perkins, K.S., Lewis, A.M., 2002. Steady-state centrifuge [simultaneous determination of water transmission and retention properties]. In: Danc, J.H., Topp, G.C. (Eds.), Methods of Soil Analysis, Part 4–Physical Methods. Soil Science Society of America, Madison, Wisconsin, p. 903–916, 933–936.

Or, D., Tuller, M., 1999. Liquid retention and interfacial area in variably saturated porous media: upscaling from single-pore to sample-scale model. Water Resour. Res. 35 (12), 3591–3605.

Pachepsky, Y.A., Rawls, W.J., 2003. Soil structure and pedotransfer functions. Eur. J. Soil Sci. 54, 443–451.

Pachepsky, Y.A., Rajkai, K., Tóth, B., 2015. Pedotransfer in soil physics: trends and outlook – a review. Agrokém. Talajtan 64 (2), 339–360.

Ramos, T.B., Horta, A., Gonçalves, M.C., Martins, J.C., Pereira, L.S., 2014. Development of ternary diagrams for estimating water retention properties using geostatistical approaches. Geoderma 230–231, 229–242.

Rivers, E.D., Shipp, R.F., 1972. Available water capacity of sandy and gravelly North Dakota soil. Soil Sci. 113, 74–80.

Rouault, Y., Assouline, S., 1998. A probabilistic approach towards modeling the relationships between particle and pore size distributions: the multicomponent packed sphere case. Powder Technol. 96 (1), 33–41.

Schaap, M.G., Leij, F.J., 1998. Using neural networks to predict soil water retention and soil hydraulic conductivity. Soil Till. Res. 47 (1–2), 37–42.

Schaap, M.G., Leij, F.J., van Genuchten, M.Th., 2001. Rosetta: a computer program for estimating soil hydraulic parameters with hierarchical pedotransfer functions. J. Hydrol. 251 (3–4), 163–176.

Schaap, M.G., Nemes, A., van Genuchten, M.Th., 2004. Comparison of models for indirect estimation of water retention and available water in surface soils. Vadose Zone J. 3 (4), 1455–1463.

Shirazi, M.A., Boersma, L., 1984. A unifying quantitative analysis of soil texture. Soil Sci. Soc. Am. J. 48 (1), 142–147.

Skaggs, T.H., Arya, L.M., Shouse, P.J., Mohanty, B.P., 2001. Estimating particle-size distribution from limited soil texture data. Soil Sci. Soc. Am. J. 65 (4), 1038–1044.

Soet, M., Stricker, J.N.M., 2003. Functional behaviour of pedotransfer functions in soil water flow simulation. Hydrol. Process. 17 (8), 1659–1670.

Tuller, M., Or, D., Dudley, L.M., 1999. Adsorption and capillary condensation in porous media: liquid retention and interfacial configurations in angular pores. Water Resour. Res. 35 (7), 1949–1964.

van Genuchten, M.Th., 1980. A closed-form equation for predicting the hydraulic conductivity of unsaturated soils. Soil Sci. Soc. Am. J. 44, 892–898.

van Genuchten, M.Th., Leij, F.J., Yates, S.R., 1991. The RETC code for quantifying the hydraulic functions of unsaturated soils. US Salinity Laboratory, USDA-ARS, Riverside, CA.

Vaz, C.M.P., de Freitas Iossi, M., de Mendonça Naime, J., Macedo, Á., Reichert, J.M., Reinert, D.J., Cooper, M., 2005. Validation of the Arya and Paris water retention model for Brazilian soils. Soil Sci. Soc. Am. J. 69 (3), 577–583.

Wösten, J.H.M., Lilly, A., Nemes, A., Le Bas, C., 1999. Development and use of a database of hydraulic properties of European soils. Geoderma 90, 169–185.

Wösten, J.H.M., Pachepsky, Y.A., Rawls, W.J., 2001. Pedotransfer functions: bridging the gap between available basic soil data and missing soil hydraulic characteristics. J. Hydrol. 251 (3–4), 123–150.

Wu, Y.Z., Huang, M.B., Gallichand, J., 2011. Transpirational response to water availability for winter wheat as affected by soil textures. Agric. Water Manage. 98 (4), 569–576.